Monthly Notices of the ROYAL ASTRONOMICAL SOCIETY

MNRAS **526,** 5911–5918 (2023) https://doi.org/10.1093/mnras/stad3019
Advance Access publication 2023 October 05

Binaries drive high Type Ia supernova rates in dwarf galaxies

James W. Johnson [1,2,3]★ Christopher S. Kochanek[1,2] and K. Z. Stanek[1,2]

[1]*Department of Astronomy, The Ohio State University, 140 W. 18th Ave., Columbus, OH 43210, USA*
[2]*Center for Cosmology and Astroparticle Physics (CCAPP), The Ohio State University, 191 W. Woodruff Ave., Columbus, OH 43210, USA*
[3]*The Observatories of the Carnegie Institution for Science, 813 Santa Barbara St., Pasadena, CA 91101, USA*

Accepted 2023 October 1. Received 2023 September 18; in original form 2022 November 8

ABSTRACT

The scaling of the specific Type Ia supernova (SN Ia) rate with host galaxy stellar mass $\dot{N}_{Ia}/M_\star \sim M_\star^{-0.3}$ as measured in ASAS-SN and DES strongly suggests that the number of SNe Ia produced by a stellar population depends inversely on its metallicity. We estimate the strength of the required metallicity dependence by combining the average star formation histories (SFHs) of galaxies as a function of their stellar mass with the mass–metallicity relation (MZR) for galaxies and common parametrizations for the SN Ia delay-time distribution. The differences in SFHs can account for only ∼30 per cent of the increase in the specific SN Ia rate between stellar masses of $M_\star = 10^{10}$ and $10^{7.2}\,M_\odot$. We find that an additional metallicity dependence of approximately $\sim Z^{-0.5}$ is required to explain the observed scaling. This scaling matches the metallicity dependence of the close binary fraction observed in APOGEE, suggesting that the enhanced SN Ia rate in low-mass galaxies can be explained by a combination of their more extended SFHs and a higher binary fraction due to their lower metallicities. Due to the shape of the MZR, only galaxies below $M_\star \approx 3 \times 10^9\,M_\odot$ are significantly affected by the metallicity-dependent SN Ia rates. The $\dot{N}_{Ia}/M_\star \sim M_\star^{-0.3}$ scaling becomes shallower with increasing redshift, dropping by factor of ∼2 at $10^{7.2}\,M_\odot$ between $z = 0$ and 1 with our $\sim Z^{-0.5}$ scaling. With metallicity-independent rates, this decrease is a factor of ∼3. We discuss the implications of metallicity-dependent SN Ia rates for one-zone models of galactic chemical evolution.

Key words: stars: supernovae – white dwarfs – galaxies: abundances – galaxies: dwarf – galaxies: evolution.

1 INTRODUCTION

Type Ia supernovae (SNe Ia) arise from the thermonuclear detonation of a white dwarf (WD; Hoyle & Fowler 1960; Colgate & McKee 1969), the exposed carbon–oxygen core of a low-mass star. SN surveys have revealed that low-mass galaxies are more efficient producers of these events than their higher mass counterparts (e.g. Mannucci et al. 2005; Sullivan et al. 2006; Li et al. 2011; Smith et al. 2012). In particular, Brown et al. (2019) found that the specific SN Ia rate – the rate per unit stellar mass – scales approximately with the inverse square root of the stellar mass itself ($\dot{N}_{Ia}/M_\star \sim M_\star^{-0.5}$) using SNe Ia from the All-Sky Automated Survey for Supernovae (ASAS-SN; Shappee et al. 2014; Kochanek et al. 2017) and assuming the Bell et al. (2003) stellar mass function (SMF). The measurement depends on the SMF because the number of observed SNe must be normalized by the number of galaxies in order to compute a specific SN rate. Consequently, the scaling becomes shallower ($\dot{N}_{Ia}/M_\star \sim M_\star^{-0.3}$) when using the steeper Baldry et al. (2012) double-Schechter SMF parametrization (Gandhi et al. 2022). This change leads to agreement between the ASAS-SN measurements and Wiseman et al.'s (2021) estimates from the Dark Energy Survey (DES; Dark Energy Survey Collaboration 2016) using their own measurements of the SMF, which closely agree with the Baldry et al. (2012) SMF. Although the exact strength of the scaling depends on the SMF, it is clear that the specific SN Ia rate is higher in dwarf galaxies. There are a handful of potential pathways that could give rise to this empirical result.

First, the mean star formation histories (SFHs) of galaxies vary with the stellar mass of the system. In semi-analytic models of galaxy formation (see e.g. the reviews of Baugh 2006 and Somerville & Davé 2015), dwarf galaxies in the field have more extended SFHs than their higher mass counterparts. This mass dependence is also seen in hydrodynamical simulations of galaxy formation (e.g. Garrison-Kimmel et al. 2019). Since SN Ia delay-time distributions (DTDs) decline with age (e.g. Greggio 2005; Maoz & Mannucci 2012), galaxies with more recent star formation should have higher specific SN Ia rates.

Secondly, Kistler et al. (2013) argued that the dependence of the specific SN Ia rate on stellar mass may be driven by metallicity. Lower mass galaxies host lower metallicity stellar populations (Gallazzi et al. 2005; Kirby et al. 2013; Simon 2019) and lower metallicity gas reservoirs (Tremonti et al. 2004; Zahid, Kewley & Bresolin 2011; Andrews & Martini 2013; Zahid et al. 2014). Kistler et al. (2013) point out that lower metallicity stars leave behind higher mass WDs which could potentially grow to the Chandrasekhar mass and subsequently explode more easily than their less massive, high metallicity counterparts. Lower metallicity stars have weaker winds during the asymptotic giant branch phase (Willson 2000; Marigo & Girardi 2007), leading to lower mass-loss rates and more massive cores (Kalirai, Marigo & Tremblay 2014), producing more massive WDs for fixed initial mass stars at lower

★ E-mail: jjohnson10@carnegiescience.edu

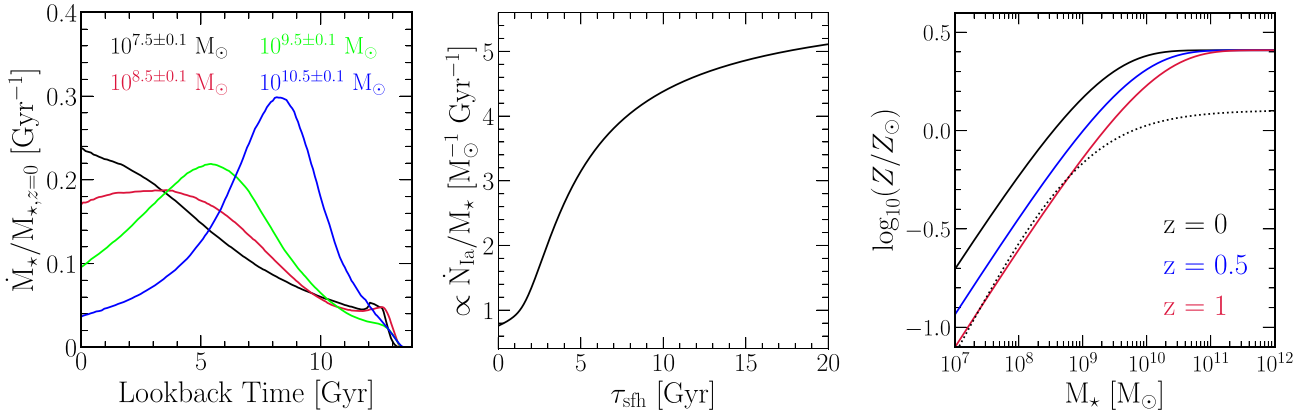

Figure 1. Left: The best-fit mean SFHs of the UNIVERSEMACHINE galaxies with present-day stellar masses of $M_\star = 10^{7.5\pm0.1}$ (black), $10^{8.5\pm0.1}$ (red), $10^{9.5\pm0.1}$ (green), and $10^{10.5\pm0.1}$M$_\odot$ (blue) normalized by their present-day stellar masses. **Middle**: The specific SN Ia rate as a function of the e-folding time-scale of the SFH τ_{sfh} assuming a linear-exponential time dependence and a τ^{-1} power-law SN Ia DTD. **Right**: The redshift-dependent MZR reported by Zahid et al. (2014) at $z = 0$ (black solid), $z = 0.5$ (blue), and $z = 1$ (red). For comparison, we include the $z \approx 0$ MZR measured by Andrews & Martini (2013; black dotted).

metallcity (Umeda et al. 1999; Meng, Chen & Han 2008; Zhao et al. 2012).

Furthermore, in both the single (e.g. Whelan & Iben 1973) and double degenerate scenarios (e.g. Iben & Tutukov 1984; Webbink 1984), SNe Ia arise in binary systems. Based on multiplicity measurements of solar-type stars from the Apache Point Observatory Galaxy Evolution Experiment (APOGEE; Majewski et al. 2017), Badenes et al. (2018) and Moe, Kratter & Badenes (2019) find that the stellar close binary fraction increases toward low metallicities. Consequently, dwarf galaxies should have more potential SN Ia progenitors per unit mass of star formation due to more massive WDs and a higher close binary fraction. Motivated by these results, Gandhi et al. (2022) explore a handful of parametrizations for the metallicity dependence of the SN Ia rate in re-simulated galaxies from FIRE-2 (Hopkins et al. 2018). They find that a $Z^{-0.5}$ scaling where Z is the metallicity leads to better agreement with the empirical relationship between galactic stellar masses and stellar abundances than when using metallicity-independent SN Ia rates.

In this paper, we assume that the strong scaling of the specific SN Ia rate with stellar mass is due to metallicity and conduct simple numerical calculations to investigate its origin. We combine the mean SFHs of galaxies at fixed stellar mass from the UNIVERSEMACHINE semi-analytic model (Behroozi et al. 2019) and the popular τ^{-1} SN Ia DTD (e.g. Maoz & Mannucci 2012) with the mass–metallicity relation (MZR) for galaxies (Tremonti et al. 2004; Zahid et al. 2011; Andrews & Martini 2013; Zahid et al. 2014). Given the mean SFH and DTD, we can compute the characteristic SN Ia rate for galaxies of a given stellar mass, and by assuming that they lie along the observed MZR, we can include various scalings of the rate with metallicity. We describe the model in Section 2 and the effect on Type Ia rates in Section 3. In Section 4, we present simple models exploring the consequences of metallicity-dependent SN Ia rates for galactic chemical evolution models. We summarize our findings in Section 5.

2 GALACTIC PROPERTIES

We begin by examining how the mean galactic SFH varies with present-day stellar mass as predicted by the UNIVERSEMACHINE semi-empirical model (Behroozi et al. 2019). While conventional semi-analytic models forward model galaxy formation (see e.g. the review in Somerville & Davé 2015), UNIVERSEMACHINE uses dark matter halo properties from the *Bolshoi-Planck* and *Multi-Dark Planck 2* dark matter only simulations (Klypin et al. 2016) to fit continuity equations to the observations. It successfully reproduces a broad range of well-constrained observables, including SMFs, cosmic SFRs, specific SFRs, quenched fractions, and UV luminosity functions. While some semi-analytic models have used the extended Press–Schechter formalism (Press & Schechter 1974; Bond et al. 1991) to generate halo merger trees and push the lower stellar mass limit of their model down to $M_\star \approx 10^7$ M$_\odot$ (e.g. Somerville, Popping & Trager 2015), an advantage of UNIVERSEMACHINE is that the high mass resolution of the *Bolshoi-Planck* and *Multi-Dark Planck 2* simulations allows merger trees down to $M_\star = 10^{7.2}$ M$_\odot$ to be obtained directly from the simulations. Conveniently, this limit is approximately the lowest mass for which there are empirical constraints on the specific SN Ia rate from ASAS-SN (Brown et al. 2019) and DES (Wiseman et al. 2021), though one source of uncertainty is that UNIVERSEMACHINE's constraints on SFHs at these masses involve significant extrapolation. To relate these predictions to data from the untargeted ASAS-SN survey (Shappee et al. 2014; Kochanek et al. 2017), we take the full galaxy sample from UNIVERSEMACHINE, including both star forming and quenched galaxies as well as both centrals and satellites, though centrals are the dominant population across the full stellar mass range.

In the left panel of Fig. 1, we show the best-fitting mean SFH as a function of lookback time in four narrow bins of present day stellar mass. In general, low stellar mass galaxies have more extended SFHs than their higher mass counterparts. This effect is sufficiently strong that for stellar masses of $\sim 10^{7.5}$ M$_\odot$, typical SFRs are still increasing at the present day, while $\sim 10^{10.5}$ M$_\odot$ galaxies experienced their fastest star formation long ago.

We adopt a DTD that scales with the age of a stellar population as τ^{-1} starting at a delay time $t_D = 100$ Myr as suggested by comparisons of the cosmic SFH with the volumetric SN Ia rate as a function of redshift (Maoz & Mannucci 2012; Maoz, Mannucci & Brandt 2012; Graur & Maoz 2013; Graur et al. 2014). We conducted our analysis using alternative choices of the power-law index as

well as an exponential DTD with an e-folding time-scale of $\tau_{\rm Ia} = 1.5\,{\rm Gyr}$ and found similar conclusions in all cases. We do not consider metallicity-dependent variations in the shape of the DTD here, instead focusing on the overall normalization. In principle, the minimum delay of the DTD could be as short as ∼40 Myr if WDs are produced by $\lesssim 8\,{\rm M}_\odot$ stars (e.g. Hurley, Pols & Tout 2000), and perhaps even shorter at low metallicity if the total metal content of a star significantly impacts its lifetime (e.g. Kodama & Arimoto 1997; Vincenzo et al. 2016). However, if SNe Ia require some additional time following WD formation, the minimum delay will be longer. Since we are interested in the first-order effects of variations in the SFH on specific SN Ia rates, we assume a value of $t_{\rm D} = 100\,{\rm Myr}$. In calculations using both $t_{\rm D} = 40$ and 150 Myr, we found similar results.

For an SFH $\dot{M}_\star$ and DTD $R_{\rm Ia}$ as functions of lookback time τ, the specific SN Ia rate at a stellar mass $M_\star$ is

$$\frac{\dot{N}_{\rm Ia}(M_\star|\gamma)}{M_\star} \propto Z(M_\star)^\gamma \frac{\int_0^{T-t_{\rm D}} \dot{M}_\star(\tau|M_\star) R_{\rm Ia}(\tau){\rm d}\tau}{\int_0^T \dot{M}_\star(\tau|M_\star){\rm d}\tau} \quad (1)$$

where $T = 13.2\,{\rm Gyr}$ is the time elapsed between the onset of star formation and the present day. To investigate the effects of metallicity, we add a power-law metallicity scaling $Z(M_\star)^\gamma$ where Z is given by the MZR. In detail, the WDs producing SNe Ia come from stellar populations with a distribution of metallicities, and therefore a more accurate parametrization would marginalize $Z(M_\star)^\gamma$ over each galaxy's enrichment history. The inferred rates would be higher if one were to account for this effect, but the event rate in low-mass field galaxies should be dominated by young stellar populations anyway due to their tendency to form at low redshift combined with the steepness of the SN Ia DTD. Accounting for distributions in metallicity can be addressed by either including an MZR that evolves with redshift inside the integral or folding in some model of galactic chemical evolution (GCE; see e.g. Section 4 below or the review by Matteucci 2021). We are only interested in the scaling of the rates with $M_\star$, so we normalize all rates to unity at $M_\star = 10^{10}\,{\rm M}_\odot$ following Brown et al. (2019). Although the denominator of equation (1) in detail should depend on mass-loss from stars as they eject their envelopes, this is an approximately constant term which can safely be neglected in the interest of computing relative rates (≈40 per cent for a Kroupa 2001 IMF; see discussion in sections 2.2 and 3.7 of Weinberg, Andrews & Freudenburg 2017).

To qualitatively illustrate how the specific SN Ia rate scales with the time-scale over which star formation occurs, we consider the simple example of a linear-exponential parametrization $\dot{M}_\star \propto t e^{-t/\tau_{\rm sfh}}$ where $t = T - \tau$. The middle panel of Fig. 1 shows equation (1) as a function of the e-folding time-scale $\tau_{\rm sfh}$ assuming $\gamma = 0$. The specific SN Ia rate is lowest in the limiting case of a single episode of star formation (i.e. $\tau_{\rm sfh} \to 0$), rises steeply until $\tau_{\rm sfh} \approx 10\,{\rm Gyr}$, and then flattens once $\tau_{\rm sfh} \gtrsim T$. A higher specific SN Ia rate as observed in dwarf galaxies is therefore a natural consequence of their more extended SFHs, though we demonstrate below that this effect accounts for only a factor of ∼2 increase in the rate between $10^{7.2}$ and $10^{10}\,{\rm M}_\odot$.

The right panel of Fig. 1 shows the MZR parametrized by Zahid et al. (2014; see their equation 5)[1] at redshifts $z = 0$, 0.5 and 1 in comparison to the Andrews & Martini (2013) parametrization at $z = 0$. Although UNIVERSEMACHINE allows us to investigate these effects at stellar masses as low as $10^{7.2}\,{\rm M}_\odot$, the Zahid et al. (2014) measurements are available only for $M_\star \approx 10^9$–$10^{11}\,{\rm M}_\odot$ galaxies. Andrews & Martini (2013) used stacked spectra from the Sloan Digital Sky Survey (SDSS; York et al. 2000) to obtain direct measurements of the oxygen abundance in bins of stellar mass extending as low as $\sim 10^{7.4}\,{\rm M}_\odot$. Relative to Zahid et al. (2014), the Andrews & Martini (2013) parametrization has a lower plateau but otherwise a similar slope and turnover mass. Because we simply normalize the rates to unity at $M_\star = 10^{10}\,{\rm M}_\odot$, only the shape of the MZR matters, and we find similar results using both parametrizations. UNIVERSEMACHINE includes the parametrization of metallicities as a function of stellar mass and redshift from Maiolino et al. (2008), which is similar in shape to Andrews & Martini (2013) and Zahid et al. (2014). In order to estimate SN Ia rates at redshifts of $z = 0.5$ and $z = 1$, we use the redshift-dependent Zahid et al. (2014) formalism in Section 3. Although these MZRs are similarly shaped, there are others in the literature that are different, particularly at the low-mass end where the measurements are more challenging (see e.g. the review by Kewley, Nicholls & Sutherland 2019).

Given a present-day stellar mass, we compute its SFH as a function of lookback time by interpolating between the stellar mass and snapshot times included in the UNIVERSEMACHINE predictions. We then compute the specific SN Ia rate according to equation (1) given the implied SFH and and a τ^{-1} DTD, amplifying the rate by a factor of Z^γ where the metallicity Z is computed from the Zahid et al. (2014) MZR. Because these calculations are simply using the UNIVERSEMACHINE SFHs, our predictions are unaffected by the SMF dependence of the observational estimates (i.e. equation (1) can simply be divided by $M_\star$ as opposed to an integral over the SMF). However, the UNIVERSEMACHINE SFHs are still dependent on the Baldry et al. (2012) SMF, because they use this form as an empirical constraint at $z = 0$. Comparing our predictions to scalings of the SN Ia rate with masses derived from a different SMF would require updated SFHs.

The *stellar* MZR (e.g. Gallazzi et al. 2005; Kirby et al. 2013; Simon 2019) is perhaps a better relation to use than the gas-phase MZR since the stellar populations produce the SN events. However, given the uncertainties involved, the gas-phase measurements should be accurate enough for a first investigation into possible origins of metallicity dependent SN Ia rates. While Moe et al.'s (2019) metallicity dependence of the close binary fraction is based on stellar Fe abundances, we use gas-phase O abundances since this observable is the primary focus of population studies of galaxy metallicities in terms of both models and measurements. While the O and Fe abundances of stellar populations are correlated, the relationship between the two is not linear due to the evolving contributions of massive stars and SNe Ia (see e.g. Section 4). Moreover, binarity appears to depend on both [Fe/H] and [α/Fe] (Mazzola et al. 2020). The underlying multiplicity measurements are also challenging (Moe & Di Stefano 2017; Offner et al. 2022) but will improve in the coming years thanks to the expansion of available data (e.g. SDSS-V; Kollmeier et al. 2017).

[1] We have transformed from their $\log_{10}$(O/H) measurements to the logarithmic abundance relative to the Sun $\log_{10}(Z/Z_\odot)$ assuming the solar oxygen abundance derived by Asplund et al. (2009).

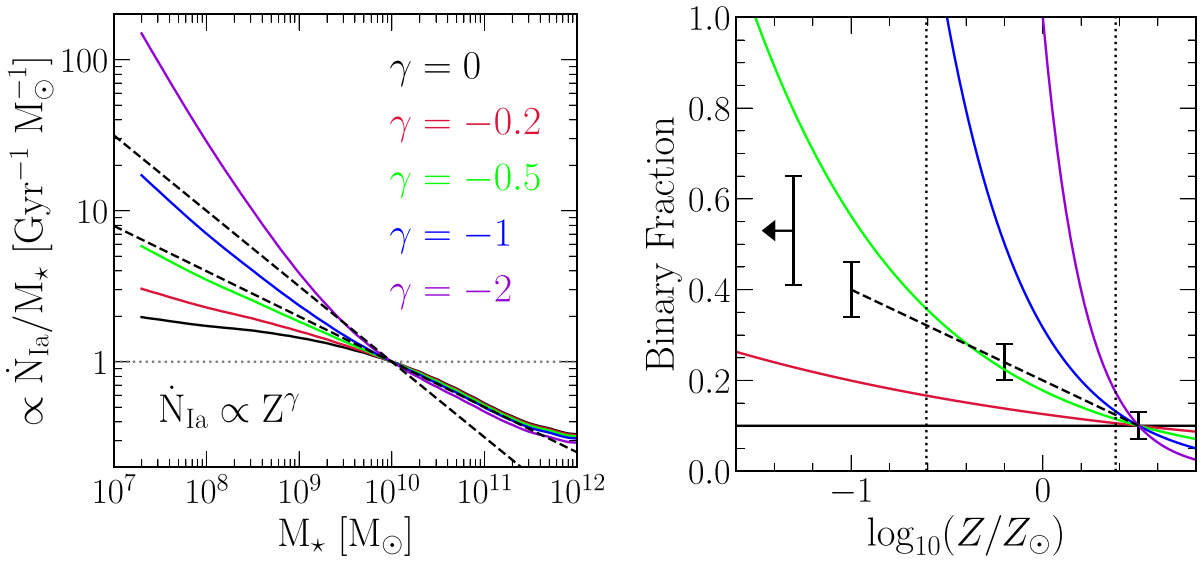

Figure 2. Left: Predicted scalings of the specific SN Ia rate with galaxy stellar mass (see equation (1)) assuming the mean UNIVERSEMACHINE SFHs and a single power-law Z^γ metallicity-dependence with $\gamma = 0$ (i.e. no dependence; black), $\gamma = -0.2$ (red), $\gamma = -0.5$ (green), $\gamma = -1$ (blue), and $\gamma = -2$ (purple). Following Brown et al. (2019) and Gandhi et al. (2022), we normalize all rates to a value of 1 at $M_\star = 10^{10}\,M_\odot$. Black dashed lines denote the scalings of $\dot{N}_{Ia}/M_\star \sim M_\star^{-0.5}$ and $\dot{N}_{Ia}/M_\star \sim M_\star^{-0.3}$ derived when normalizing the observed rates by the Bell et al. (2003) and Baldry et al. (2012) SMFs, respectively. **Right**: The same metallicity scalings as in the left panel in comparison to the close binary fractions observed in APOGEE (Moe et al. 2019; black dashed line with error bars) normalized to the observed binary fraction of 10 per cent at $\log_{10}(Z/Z_\odot) = +0.5$. The characteristic metallicities of $M_\star = 10^{7.2}\,M_\odot$ ($\log_{10}(Z/Z_\odot) \approx -0.6$) and $10^{10}\,M_\odot$ galaxies ($\log_{10}(Z/Z_\odot) \approx +0.4$) are marked with black dotted lines. The arrow denotes the binary fraction of 53 ± 12 per cent measured by Moe et al. (2019) at [Fe/H] $= -3$.

Lastly, changes in SN rates will impact the feedback into the interstellar medium, and by extension the SFH, so the post-processing prescription of equation (1) is somewhat oversimplified (Gandhi et al. 2022). None the less, it should suffice for understanding the first-order effects of metallicity-dependent SN Ia rates.

3 PREDICTED SN IA RATES

The left panel of Fig. 2 shows the specific SN Ia rate for several choices of γ in comparison to the $\dot{N}_{Ia}/M_\star \sim M_\star^{-0.5}$ and $\dot{N}_{Ia}/M_\star \sim M_\star^{-0.3}$ scalings of the observed rate with the Bell et al. (2003) and Baldry et al. (2012) SMFs, respectively. The metallicity dependence has a significant impact only below $M_\star \approx 3 \times 10^9\,M_\odot$ due to the shape of the MZR; this is the mass above which the MZR flattens considerably (see Fig. 1). Assuming no metallicity dependence (i.e. $\gamma = 0$), these calculations suggest that the variations in SFHs between $\sim 10^{7.2}$ and $\sim 10^{10}\,M_\odot$ can account for only a factor of $\sim$2 increase in the specific SN Ia rate. The $\gamma = -0.5$ case is generally consistent with a mass dependence of $M_\star^{-0.3}$, while the steeper dependence of $M_\star^{-0.5}$ would require a stronger scaling of roughly $\gamma \approx -1.5$.

In the right panel of Fig. 2, we compare the same scalings to the close binary fractions in APOGEE measured by Moe et al. (2019). The binary fraction must eventually saturate, along with its impact on SN rates, and Moe et al. (2019) measured 53 ± 12 per cent in the most metal-poor stars ([Fe/H] ≈ -3), which we also include in Fig. 2. However, our sample does not extend to such low metallicities. The line at $Z \approx 10^{-0.6}\,Z_\odot$ is the characteristic abundance of an $M_\star = 10^{7.2}\,M_\odot$ galaxy in the Zahid et al. (2014) parametrization. For the range of metallicities spanned by the stellar masses we explore here, the close binary fraction is remarkably consistent with a $\gamma = -0.5$ scaling with metallicity. If one instead takes $Z \approx 0.1\,Z_\odot$ for a $\sim 10^{7.2}\,M_\odot$ galaxy as suggested by Andrews & Martini (2013), then there is a slight tension between a $\gamma = -0.5$ scaling and the close binary fraction measured by Moe et al. (2019). That is, although the normalization of the MZR does not impact our predicted scaling of the specific SN Ia rate with stellar mass, it does impact whether or not binarity can explain the effect across the full range of metallicities. In particular, the stellar MZR has a lower normalization (e.g. Gallazzi et al. 2005; Kirby et al. 2013; Simon 2019), reaching [Fe/H] ≈ -1 at $\sim 2 \times 10^8\,M_\odot$. Comparing this normalization with Moe et al.'s (2019) measurement at [Fe/H] ≈ -3 suggests that variations in binarity may be minimal in the 10^7–$10^8\,M_\odot$ range and that additional effects would be required to explain a steep increase in SN Ia rates with decreasing mass.

There is some additional freedom to adjust the metallicity dependence beyond that of binaries, so the agreement need not be perfect. For example, any additional increase in the SN Ia rates not supplied by an increased binary fraction could arise due to more massive WDs forming at low Z – the scenario postulated by Kistler et al. (2013). None the less, it appears that the scaling of the close binary fraction with metallicity can explain the majority of the effect if the rate scales with mass as $\dot{N}_{Ia}/M_\star \sim M_\star^{-0.3}$. If, instead, the $\sim M_\star^{-0.5}$ scaling found using the Bell et al. (2003) SMF is accurate, then the required $\gamma \approx -1.5$ scaling cannot be explained by the close binary fraction alone as it would reach unphysical values (> 1) within the range of observed metallicities.

Due to the evolution of the MZR, the mass dependence of the specific SN Ia rate at different redshifts could empirically distinguish between $\gamma = 0$ and $\gamma = -0.5$. To investigate this possibility, we simply evaluate equation (1) over the appropriate range of lookback time assuming standard cosmological parameters (Planck Collaboration et al. 2014). For the $\gamma = 0$ case, we also show the effect of applying an additional $(M_\star/10^{10}\,M_\odot)^{-0.15}$. This pre-factor brings the $\gamma = 0$

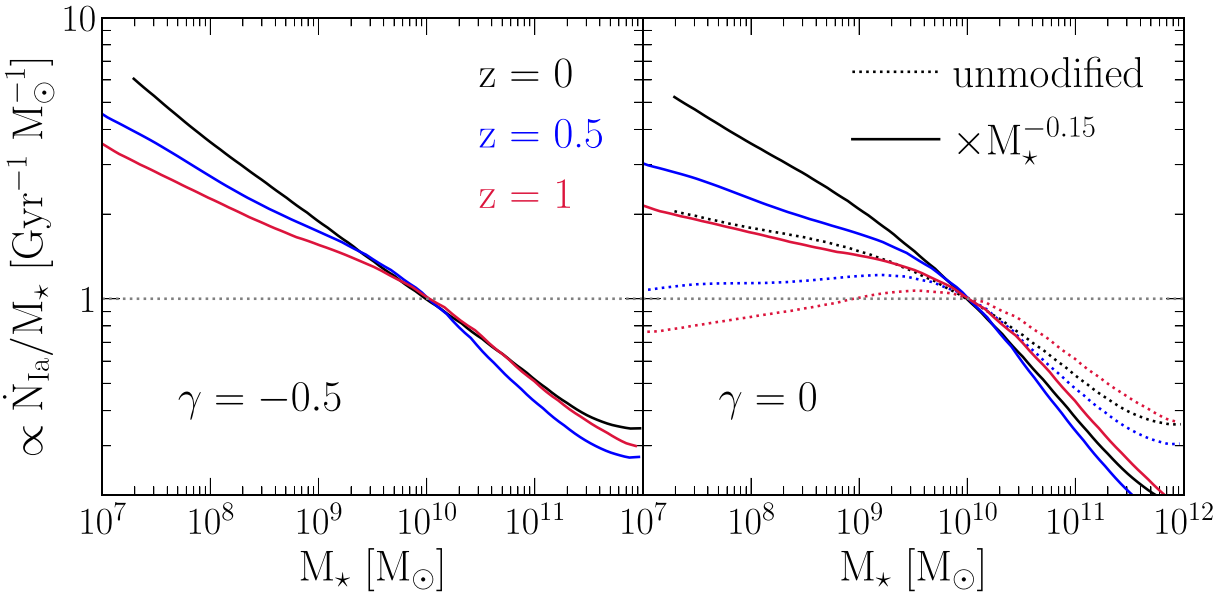

Figure 3. The specific SN Ia rate normalized to 1 at 10^{10} M$_\odot$ as a function of stellar mass with ($\gamma = -0.5$, left) and without a metallicity dependence ($\gamma = 0$, right) at redshifts $z = 0$ (black), 0.5 (blue), and 1 (red). In the right panel, we artificially scale the rates by a factor of $(M_\star/10^{10}\,\mathrm{M}_\odot)^{-0.15}$ to bring the $z = 0$ predictions into better agreement with an $\sim \mathrm{M}_\star^{-0.3}$ scaling as predicted by the $\gamma = -0.5$ case. Stellar masses correspond to the appropriate redshift (i.e. the rates for $z = 1$, use the $z = 1$ stellar masses and not the present-day stellar masses). We show the unmodified rates as dotted lines (the black solid line in the left panel and the black dotted line in the right panel are the same as the green line and black solid line in the left panel of Fig. 2, respectively).

predictions into better agreement with the empirical $\dot{\mathrm{N}}_{\mathrm{Ia}}/\mathrm{M}_\star \sim \mathrm{M}_\star^{-0.3}$ scaling at $z = 0$ and is intended to encapsulate the mass scaling needed for some other unknown process to sufficiently amplify the SN Ia rate at low stellar masses if it is instead not due to metallicity effects.

We show the resulting specific SN Ia rates as a function of stellar mass at $z = 0$, 0.5, and 1 in Fig. 3. In both the $\gamma = 0$ and $\gamma = -0.5$ cases, the scaling of the specific SN Ia rate with galaxy stellar mass becomes shallower with increasing redshift. If $\gamma = -0.5$, these calculations suggest that it should decrease by a factor of $\sim$2 between $z = 0$ and $z = 1$ at $M_\star \approx 10^{7.2}\,\mathrm{M}_\odot$, the lowest stellar mass for which we have made predictions at all three redshifts. If $\gamma = 0$, then the rate instead decreases by a factor of $\sim$3 at $\sim 10^{7.2}\,\mathrm{M}_\odot$. This difference arises because the metallicities of dwarf galaxies decrease with increasing redshift and $\gamma = -0.5$ allows them to sustain higher SN Ia rates than if $\gamma = 0$. Empirically, the cosmic SN Ia rate increases with redshift (e.g. Graur et al. 2014), and we have verified that our framework reproduces this result by integrating over the SMF (similar to equation 3 below). Given this result and the lower stellar masses of the host galaxies at high redshift, one might expect the trend to steepen with increasing z. The slope instead decreases here because the lines in Fig. 3 (right panel) are moving to the right with time as galaxies grow in mass, and we normalize to unity at a stellar mass of $10^{10}\,\mathrm{M}_\odot$ at all redshifts.

While empirical measurements of the specific SN Ia rate as a function of stellar mass depend on the assumed SMF (Gandhi et al. 2022), the host galaxy mass distribution of observed events does not, making it a potentially more observationally feasible diagnostic. As noted in Fig. 2, only dwarf galaxies are significantly affected by a metallicity-dependent scaling of SN Ia rates due to the shape of the MZR, so a $\gamma \approx -0.5$ scaling should appear as an enhanced SN Ia rate at the low-mass end of the distribution. Although this empirical measurement does not depend on the SMF, our theoretical prediction

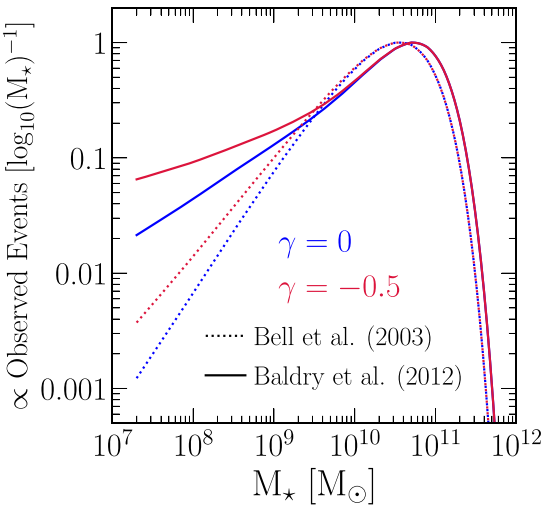

Figure 4. The predicted stellar mass distribution of $z = 0$ SN Ia host galaxies in an untargeted survey (see equation 3) with the Bell et al. (2003; dotted) and Baldry et al. (2012; solid) SMFs for both metallicity-dependent ($\gamma = -0.5$, red) and metallicity-independent rates ($\gamma = 0$, blue). All distributions are normalized to a maximum value of 1.

does because we must take into account the relative abundances of galaxies of different stellar masses. The observed rate in a bin of stellar mass can be expressed as the product of the characteristic rate $\dot{\mathrm{N}}_{\mathrm{Ia}}$ at a given stellar mass and the integral of the SMF $\Phi(M_\star)$ over the bin in stellar mass,

$$\dot{N}_{\mathrm{Ia,cosmic}}(M_\star|\gamma) = \dot{N}_{\mathrm{Ia}}(M_\star|\gamma) \int_{M_\star}^{M_\star + dM_\star} \Phi(M_\star)\mathrm{d}M_\star, \quad (3)$$

where $\dot{\mathrm{N}}_{\mathrm{Ia}}$ is the numerator of equation (1). We show this distribution in Fig. 4 for each combination of $\gamma = 0$ and -0.5 and the Bell et al. (2003) and Baldry et al. (2012) SMFs, normalizing to a maximum

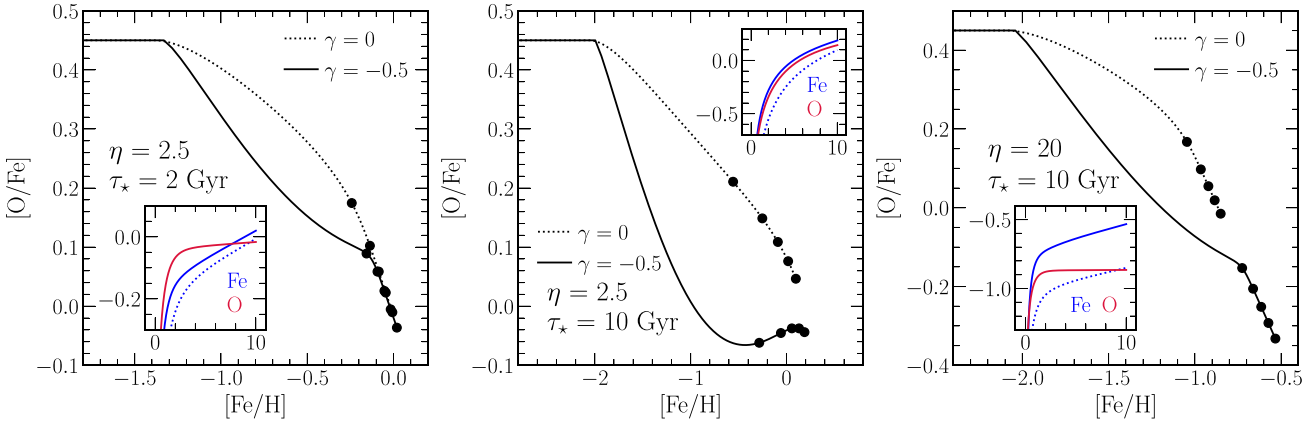

Figure 5. A comparison of one-zone galactic chemical evolution models based on Johnson & Weinberg (2020, for details, see their section 2) with ($\gamma = -0.5$, solid) and without ($\gamma = 0$, dotted) metallicity-dependent SN Ia rates. Tracks denote the O and Fe abundances in the interstellar medium parametrized as a function of time with points marked at $T = 2$, 4, 6, 8, and 10 Gyr. Insets illustrate [O/H] and [Fe/H] as a function of time in Gyr for the corresponding model. We note on each panel the choice of the outflow mass-loading factor η and the star formation efficiency time-scale $\tau_\star$.

value of unity. For untargeted surveys like ASAS-SN, equation (3) should describe the observed host galaxy stellar mass distribution exactly, whereas targeted surveys like the Lick Observatory SN Search (LOSS; Li et al. 2000; Filippenko et al. 2001) would need to correct for their target galaxy selection criteria.

Fig. 4 shows that galaxies with stellar masses of $M_\star = 10^{10}$–$10^{11}\,\mathrm{M}_\odot$ should dominate the SN Ia rate for all choices of the SMF and γ. This peak rate simply represents the galaxies that dominate the stellar mass. For a given choice of the SMF, $\gamma = -0.5$ increases the number of SNe Ia at $M_\star \approx 10^{7.2}\,\mathrm{M}_\odot$ by a factor of $\sim$3 relative to $\gamma = 0$. However, Fig. 4 also shows that the enhancement is small compared to the differences between the two SMFs. Between the peak and $10^{7.2}\,\mathrm{M}_\odot$, the Bell et al. (2003) host mass distribution drops by $\sim$2.5 orders of magnitude while that of Baldry et al. (2012) drops by $\sim$1.5 orders of magnitude. This difference illustrates the need for precise knowledge of the SMF to accurately determine the metallicity-dependence of SN Ia rates.

4 GALACTIC CHEMICAL EVOLUTION

The realization that SN Ia rates likely depend on metallicity with a $\gamma = -0.5$ dependence has important implications for GCE models, which typically assume metallicity-independent rates. To demonstrate this, we briefly explore several one-zone models based on Johnson & Weinberg (2020) which predict the evolution of O (produced only in massive stars) and Fe (produced in both massive stars and SNe Ia). We use an exponential SFH with an e-folding time-scale of $\tau_{\rm sfh} = 6$ Gyr and a minimum delay of $t_{\rm D} = 100$ Myr before the onset of SNe Ia from a given stellar population. For metallicity-dependent rates, we simply apply a $(Z/\mathrm{Z}_\odot)^{-0.5}$ prefactor to their Fe yield of $y^{\rm Ia}_{\rm Fe} = 0.0017$, which assumes that the shape of the DTD does not vary with metallicity – only the normalization. Otherwise, these models are the same as Johnson & Weinberg (2020).

Fig. 5 illustrates the predictions of this SFH with $(\eta, \tau_\star) = (2.5, 2\,\mathrm{Gyr})$, $(2.5, 10\,\mathrm{Gyr})$, and $(20, 10\,\mathrm{Gyr})$ where $\eta \equiv \dot{M}_{\rm out}/\dot{M}_\star$ is the mass-loading factor describing the efficiency of outflows and $\tau_\star \equiv M_{\rm gas}/\dot{M}_\star$ is the inverse of the star formation efficiency. These values are appropriate for the Solar neighbourhood with efficient (left panel) and inefficient (middle panel) star formation and for a dwarf galaxy (right panel). In all cases, $\gamma = -0.5$ predicts a much more abrupt descent from the high [O/Fe] plateau because of the higher Fe yield at low metallicity. If incorporated into GCE models, this could impact the inferred evolutionary time-scales of the thick disc, known to host many of the high [O/Fe] stars in the Milky Way (Hayden et al. 2017). When the equilibrium abundance is near-Solar but star formation is slow (middle panel), the model predicts a 'secondary plateau' in [O/Fe] because the Fe enrichment rate slows down due to the metallicity-dependence of the yield (see inset). This is a noteworthy theoretical prediction because generally [α/Fe] and [Fe/H] reach equilibrium at similar times and no secondary plateau arises (e.g. Weinberg et al. 2017).

These models are intended to be illustrative rather than quantitative. In general, the only regions of chemical space where $\gamma = 0$ and $\gamma = -0.5$ agree are at near-Solar abundances and along the high [O/Fe] plateau, which occurs before the onset of SN Ia enrichment. A $\gamma = -0.5$ scaling has the strongest impact at low Z, where the metallicity-dependence of the yield shifts the Fe abundances by $\sim$0.5 dex in this example.

5 DISCUSSION AND CONCLUSIONS

Building on LOSS (Li et al. 2011), Brown et al. (2019) and Wiseman et al. (2021) found that SN Ia rates rise steeply toward low stellar mass. The exact slope depends on the adopted SMF, with $\dot{\mathrm{N}}/\mathrm{M}_\star \sim \mathrm{M}_\star^{-0.3}$ for Baldry et al. (2012) and $\dot{\mathrm{N}}/\mathrm{M}_\star \sim \mathrm{M}_\star^{-0.5}$ for Bell et al. (2003). To explain this scaling with mass, we use the mean SFHs of galaxies predicted by the UniverseMachine (Behroozi et al. 2019) semi-empirical model of galaxy formation, a standard τ^{-1} DTD (e.g. Maoz & Mannucci 2012), and the empirical MZR as parametrized by Zahid et al. (2014) to relate stellar mass to metallicity and build-in a Z^γ SN Ia rate dependence. Our results depend only on the shape of the MZR and not its absolute calibration. While lower mass galaxies have younger stellar populations, we find that this accounts for only a factor of $\sim$2 increase in the specific rate between $M_\star = 10^{7.2}$ and $10^{10}\,\mathrm{M}_\odot$. We can match the $\mathrm{M}_\star^{-0.3}$ increase if $\gamma \approx -0.5$, but $\gamma \approx -1.5$ is required to explain the steeper $\dot{\mathrm{N}}/\mathrm{M}_\star \sim \mathrm{M}_\star^{-0.5}$ scaling.

A scaling of $\gamma = -0.5$ is in excellent agreement with the dependence of the close binary fraction measured in APOGEE, which increases from $\sim$10 per cent at $\sim 3\mathrm{Z}_\odot$ to $\sim$40 per cent at $\sim 0.1\mathrm{Z}_\odot$ (Moe et al. 2019). This close match suggests that if a scaling of $\dot{\mathrm{N}}_{\rm Ia}/\mathrm{M}_\star \sim \mathrm{M}_\star^{-0.3}$ is accurate, then the elevated SN Ia rates in dwarf galaxies can be explained by a combination of their more extended

SFHs and an increased binary fraction compared to their higher mass counterparts due to differences in metallicity. While Gandhi et al. (2022) motivate their investigation from this viewpoint, here we take this argument one step further and postulate that this accounts for the majority of the increase in the specific SN Ia rate because the binary fraction can naturally account for a factor of ∼3 increase over the ∼1 decade in metallicity spanned by $M_\star = 10^{7.2}$–10^{10} $M_\odot$ galaxies. Due to the uncertainties involved (see discussion at the end of Section 2), we do not rule out the possibility of additional effects, such as the higher masses of WDs originating from lower metallicity populations (Kistler et al. 2013). These effects must be important if the steeper $\sim M_\star^{-0.5}$ scaling inferred with the Bell et al. (2003) SMF is accurate. None the less, binarity offers a natural and attractive explanation of the observed rates since SNe Ia arise from binary systems, and it can easily be the dominant effect given recent multiplicity measurements and popular choices of the MZR.

At first glance, an inverse dependence of SN Ia rates on metallicity may seem at odds with the results in Holoien et al. (2022) finding that dwarf galaxy hosts of ASAS-SN SNe Ia tend to be oxygen-rich relative to similar mass galaxies. However, SN hosts are likely not a representative sample of the underlying galaxy population, because the steeply declining DTD (e.g. Maoz & Mannucci 2012) means that the intrinsically highest SN Ia rates at any mass should be in systems which experienced a recent starburst ($\lesssim$1 Gyr ago). Since oxygen is produced by massive stars with short lifetimes (e.g. Hurley et al. 2000; Johnson 2019), these galaxies should also have a higher-than-average oxygen abundance (see e.g. Johnson & Weinberg 2020). In other words, SN Ia hosts at fixed mass should be more metal-rich than the average galaxy.

The calculations we have presented here are simplified in several regards. We assumed the characteristic SFH predicted by a model of galaxy formation at all stellar masses. Our parametrization of the MZR includes no intrinsic scatter, and taking the Zahid et al. (2014) MZR at face value for use in a power-law scaling implicitly assumes that all SNe Ia arise from stellar populations near the gas-phase abundance. Although in principle galaxies populate distributions of finite width in each of these quantities, these approximations should be fine for the purposes of predicting average trends.

Although current surveys lack the depth required to pin down SN rates across multiple decades of stellar mass at $z = 1$, the sample sizes necessary to do so may be available from next-generation facilities. First and foremost, the Nancy Grace Roman Space Telescope (Spergel et al. 2013, 2015) will obtain large samples of SNe. Roman has excellent prospects for discovering all classes of SNe at redshifts as high as $z \gtrsim 2$ and beyond (Petrushevska et al. 2016). The difficulty in empirically constraining the specific SN Ia rate at $z \approx 1$ instead comes from uncertainties in the SMF. Even at $z = 0$, these measurements are difficult due to the flux-limited nature of most surveys and the broad range of luminosities and mass-to-light ratios spanned by galaxies (see the discussion in Weigel, Schawinski & Bruderer 2016). Between $10^{7.2}$ and 10^{10} $M_\odot$, the factors of 2 and 3 predicted by our calculations with $\gamma = -0.5$ and $\gamma = 0$ are produced by power-law indices of −0.108 and −0.170, respectively. The difference between the two (0.062) is the minimum precision required for the scaling of the SMF at the low-mass end – only slightly larger than the precision achieved by Baldry et al. (2012; ±0.05, see their fig. 13). This empirical test therefore requires at least their level of precision but at $z \approx 1$.

A metallicity dependence of $Z^{-0.5}$ strongly impacts the evolution of Fe in one-zone models of galactic chemical evolution. The considerable impact that a $\gamma = -0.5$ scaling has on the predictions indicates that evolutionary parameters inferred from one-zone model fits to multi-element abundance ratios may need revised. The strongest impact is for dwarf galaxies, where the abundances are low and the higher yields predict substantial shifts in the position of the evolutionary track in abundance space. Despite the natural explanation that a metallicity dependence offers to the observed rates, the impact on GCE is rather perplexing in that its inclusion worsens the agreement between observed abundances and typical models (see e.g. Johnson et al. 2021 or Spitoni et al. 2021 for comparison). The yields may also depend on metallicity, which could mitigate or exacerbate these effects (Gronow et al. 2021).

ACKNOWLEDGEMENTS

We are grateful to David H. Weinberg and our anonymous reviewer for valuable comments which improved this manuscript. JWJ thanks Todd A. Thompson, Jennifer A. Johnson, Adam K. Leroy, and the rest of the Ohio State University Gas, Galaxies, and Feedback group for valuable discussion. JWJ also acknowledges financial support from an Ohio State University Presidential Fellowship. CSK and KZS are supported by NSF grants AST-1814440 and AST-1908570. ASAS-SN is funded in part by the Gordon and Betty Moore Foundation through grants GBMF5490 and GBMF10501 to the Ohio State University, and also funded in part by the Alfred P. Sloan Foundation grant G-2021-14192.

Software: NUMPY (Harris et al. 2020), SCIPY (Virtanen et al. 2020), MATPLOTLIB (Hunter 2007), and ASTROPY (Astropy Collaboration 2013, 2018, 2022).

DATA AVAILABILITY

The only data in this paper are the mean SFHs of the UNIVERSEMACHINE galaxies, publicly available at https://www.peterbehroozi.com/data.html.

REFERENCES

Andrews B. H., Martini P., 2013, ApJ, 765, 140
Asplund M., Grevesse N., Sauval A. J., Scott P., 2009, ARA&A, 47, 481
Astropy Collaboration, 2013, A&A, 558, A33
Astropy Collaboration, 2018, AJ, 156, 123
Astropy Collaboration, 2022, ApJ, 935, 167
Badenes C. et al., 2018, ApJ, 854, 147
Baldry I. K. et al., 2012, MNRAS, 421, 621
Baugh C. M., 2006, Rep. Prog. Phys., 69, 3101
Behroozi P., Wechsler R. H., Hearin A. P., Conroy C., 2019, MNRAS, 488, 3143
Bell E. F., McIntosh D. H., Katz N., Weinberg M. D., 2003, ApJS, 149, 289
Bond J. R., Cole S., Efstathiou G., Kaiser N., 1991, ApJ, 379, 440
Brown J. S. et al., 2019, MNRAS, 484, 3785
Colgate S. A., McKee C., 1969, ApJ, 157, 623
Dark Energy Survey Collaboration, 2016, MNRAS, 460, 1270
Filippenko A. V., Li W. D., Treffers R. R., Modjaz M., 2001, in Paczynski B., Chen W.-P., Lemme C.eds, ASP Conf. Ser. Vol. 246, IAU Colloq. 183: Small Telescope Astronomy on Global Scales. Astron. Soc. Pac., San Francisco, p. 121
Gallazzi A., Charlot S., Brinchmann J., White S. D. M., Tremonti C. A., 2005, MNRAS, 362, 41
Gandhi P. J., Wetzel A., Hopkins P. F., Shappee B. J., Wheeler C., Faucher-Giguère C.-A., 2022, MNRAS, 516, 1941
Garrison-Kimmel S. et al., 2019, MNRAS, 489, 4574
Graur O., Maoz D., 2013, MNRAS, 430, 1746
Graur O. et al., 2014, ApJ, 783, 28
Greggio L., 2005, A&A, 441, 1055

Gronow S., Côté B., Lach F., Seitenzahl I. R., Collins C. E., Sim S. A., Röpke F. K., 2021, A&A, 656, A94
Harris C. R. et al., 2020, Nature, 585, 357
Hayden M. R., Recio-Blanco A., de Laverny P., Mikolaitis S., Worley C. C., 2017, A&A, 608, L1
Holoien T. W. S. et al., 2022, ApJ, 950, 108
Hopkins P. F. et al., 2018, MNRAS, 480, 800
Hoyle F., Fowler W. A., 1960, ApJ, 132, 565
Hunter J. D., 2007, Comput. Sci. Eng., 9, 90
Hurley J. R., Pols O. R., Tout C. A., 2000, MNRAS, 315, 543
Iben I.J., Tutukov A. V., 1984, ApJS, 54, 335
Johnson J. A., 2019, Science, 363, 474
Johnson J. W., Weinberg D. H., 2020, MNRAS, 498, 1364
Johnson J. W. et al., 2021, MNRAS, 508, 4484
Kalirai J. S., Marigo P., Tremblay P.-E., 2014, ApJ, 782, 17
Kewley L. J., Nicholls D. C., Sutherland R. S., 2019, ARA&A, 57, 511
Kirby E. N., Cohen J. G., Guhathakurta P., Cheng L., Bullock J. S., Gallazzi A., 2013, ApJ, 779, 102
Kistler M. D., Stanek K. Z., Kochanek C. S., Prieto J. L., Thompson T. A., 2013, ApJ, 770, 88
Klypin A., Yepes G., Gottlöber S., Prada F., Heß S., 2016, MNRAS, 457, 4340
Kochanek C. S. et al., 2017, PASP, 129, 104502
Kodama T., Arimoto N., 1997, A&A, 320, 41
Kollmeier J. A. et al., 2017, preprint (arXiv:1711.03234)
Kroupa P., 2001, MNRAS, 322, 231
Li W. D. et al., 2000, in Holt S. S., Zhang W. W., eds, AIP Conf. Ser. Vol. 522, Cosmic Explosions: Tenth AstroPhysics Conference. Am. Inst. Phys., New York, p. 103
Li W., Chornock R., Leaman J., Filippenko A. V., Poznanski D., Wang X., Ganeshalingam M., Mannucci F., 2011, MNRAS, 412, 1473
Maiolino R. et al., 2008, A&A, 488, 463
Majewski S. R. et al., 2017, AJ, 154, 94
Mannucci F., Della Valle M., Panagia N., Cappellaro E., Cresci G., Maiolino R., Petrosian A., Turatto M., 2005, A&A, 433, 807
Maoz D., Mannucci F., 2012, PASA, 29, 447
Maoz D., Mannucci F., Brandt T. D., 2012, MNRAS, 426, 3282
Marigo P., Girardi L., 2007, A&A, 469, 239
Matteucci F., 2021, A&A Rev., 29, 5
Mazzola C. N. et al., 2020, MNRAS, 499, 1607
Meng X., Chen X., Han Z., 2008, A&A, 487, 625
Moe M., Di Stefano R., 2017, ApJS, 230, 15
Moe M., Kratter K. M., Badenes C., 2019, ApJ, 875, 61
Offner S. S. R., Moe M., Kratter K. M., Sadavoy S. I., Jensen E. L. N., Tobin J. J., 2022, in Inutsuka S., Aikawa Y., Muto T., Tomida K., Tamura M., eds, ASP Conf. Ser., Vol. 534, Protostars and Planets VII, Astron. Soc. Pac., San Francisco, p. 275
Petrushevska T. et al., 2016, A&A, 594, A54
Planck Collaboration, 2014, A&A, 571, A16
Press W. H., Schechter P., 1974, ApJ, 187, 425
Shappee B. J. et al., 2014, ApJ, 788, 48
Simon J. D., 2019, ARA&A, 57, 375
Smith M. et al., 2012, ApJ, 755, 61
Somerville R. S., Davé R., 2015, ARA&A, 53, 51
Somerville R. S., Popping G., Trager S. C., 2015, MNRAS, 453, 4337
Spergel D. et al., 2013, preprint (arXiv:1305.5422)
Spergel D. et al., 2015, preprint (arXiv:1503.03757)
Spitoni E. et al., 2021, A&A, 647, A73
Sullivan M. et al., 2006, ApJ, 648, 868
Tremonti C. A. et al., 2004, ApJ, 613, 898
Umeda H., Nomoto K., Yamaoka H., Wanajo S., 1999, ApJ, 513, 861
Vincenzo F., Matteucci F., de Boer T. J. L., Cignoni M., Tosi M., 2016, MNRAS, 460, 2238
Virtanen P. et al., 2020, Nat. Methods, 17, 261
Webbink R. F., 1984, ApJ, 277, 355
Weigel A. K., Schawinski K., Bruderer C., 2016, MNRAS, 459, 2150
Weinberg D. H., Andrews B. H., Freudenburg J., 2017, ApJ, 837, 183
Whelan J., Iben Icko J., 1973, ApJ, 186, 1007
Willson L. A., 2000, ARA&A, 38, 573
Wiseman P. et al., 2021, MNRAS, 506, 3330
York D. G. et al., 2000, AJ, 120, 1579
Zahid H. J., Kewley L. J., Bresolin F., 2011, ApJ, 730, 137
Zahid H. J., Dima G. I., Kudritzki R.-P., Kewley L. J., Geller M. J., Hwang H. S., Silverman J. D., Kashino D., 2014, ApJ, 791, 130
Zhao J. K., Oswalt T. D., Willson L. A., Wang Q., Zhao G., 2012, ApJ, 746, 144

This paper has been typeset from a TEX/LATEX file prepared by the author.